Nano Research

Open Access

Research Article

Dynamical transition of soft porous organic nanocage: The fingerprint of water-regulated ion conduction and viscoelasticity

Linkun Cai[§], Weigang Sun[§], Wenqiang You, Jiadong Chen, Xueying Yuan, Xiupeng Chen, Xian Kong, Yuyan Lai, and Panchao Yin

State Key Laboratory of Luminescent Materials and Devices & South China Advanced Institute for Soft Matter Science and Technology, Guangdong Basic Research Center of Excellence for Energy and Information Polymer Materials, South China University of Technology, Guangzhou 510641, China

[§] *Linkun Cai and Weigang Sun contributed equally to this work.*

Cite this article: *Nano Research*, **2026**, *19*, 94908366. https://doi.org/10.26599/NR.2026.94908366

ABSTRACT: To understand the importance of water in biomacromolecules and supramolecular materials, the monodispersed 1 nm porous organic nanocage (POC) is studied for their hierarchical condensed structures and relaxation dynamics at different hydration levels. The POCs possess flexible framework and their bulks stay intrinsically in glassy state with well-defined transition temperatures (T_g) and they can be attenuated from 61 to −50 °C with glass-to-rubber transition upon the increasing of hydration levels. Two-level relaxation dynamics can be probed and the temperature dependence of their relaxation time differentiates them as cooperative backbone dynamics (α) and local groups dynamics (β). The dynamical transition of α relaxation is consistent with T_g in hydration dependence. Suggested from MD simulation, water binds to the surface amine groups of POCs and accelerate its local dynamics, leading to the activated backbone dynamics for the broadly tunable visco-elasticity and thermal hysteresis for anti-freeze property. In small-angle X-ray scattering studies, the physical denaturation of POC can be observed as collapsed molecular framework and altered solubility when heated above their T_g in salt solutions. The microscopic understanding inspires the applications of hydrated POCs for elastomers and aqueous lithium electrolyte with high ionic conductivity, chemical stability and mechanical flexibility.

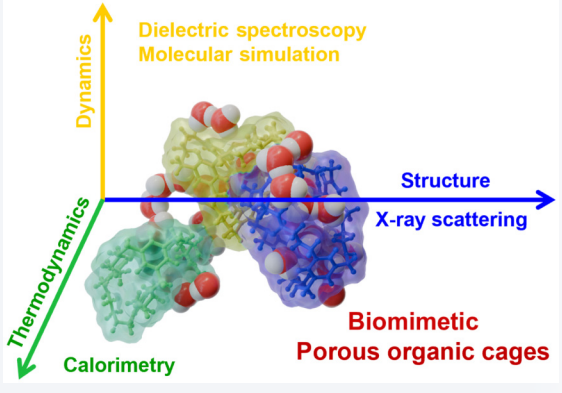

KEYWORDS: porous organic cage (POC), relaxation dynamics, nanoconfinement, supramolecular materials, glassy state

1 Introduction

Water is critical in regulating the fundamental physiological activities of biomacromolecules and soft nano-materials, from the structural role in supporting biomacromolecules and cellular framework to the vehicle role for the mass transportation across cells [1–3]. Certain functions of the biomacromolecules, e.g., mechanical flexibility and enzyme activity, are also highly dependent on the degree of hydration [4–8]. Most of the water in living systems is under the soft nanoconfinement of the cellular environment, leading to varied physicochemical properties to its bulk [9, 10]. It is inhibited to arrange into ordered crystalline structure, and remains as amorphous state even at subzero temperatures [1, 9]. That is actually the way how the antifreeze proteins (AFPs) suppress ice growth and help stabilize biology cells to survive subfreezing environment [11–13]. Meanwhile, water plays vital roles in regulating the supramolecular polymerization process not only as solvents or co-solvents, but also as co-monomers or key structural units [14, 15]. The role of water association is critical to the hierarchical structures and general functions of proteins, artificial soft nanoparticle (SNP) and supramolecular material systems and enormous experimental, simulation and theoretical efforts have been conducted [16], however, the microscopic understanding is still vague [17–19]. Their structures fluctuate constantly among several conformational substates, bringing significant difficulties in identifying the contribution of water.

To systematically probe hydration-governed dynamics in a tunable, monodisperse system, we employ porous organic cages (POCs) as nanoscale, structurally well-defined research model.

Received: October 26, 2025; **Revised:** December 20, 2025
Accepted: December 22, 2025

✉Address correspondence to yinpc@scut.edu.cn

POCs are a group of sub-5 nm, shape-persistent molecular SNPs with well-defined framework structures from the precise covalent crosslinking of multiple organic molecules [20, 21]. They possess enriched permanent micro-cavities and porosities, leading to intense research interest for host-guest chemistry and separation and purification technology [20, 22]. Generally, the linkage bonds are polar groups while the rest of the POC framework are hydrophobic, endowing the amphipathic features that enable the complex modes of inter-POC interaction and POC/water association [23–25]. Water molecules can reversibly reside in POC cavities and the channels stacked from POCs [20, 25]. In this work, POCs are applied as model system for the microscopic understanding of the structure-property relationship of proteins and SNPs. The POC1 with flexible framework and amine linkages (Fig. 1(a)) demonstrates ice recrystallization inhibition (IRI) activity when treated under humid environment and it delivers varied visco-elasticity at different hydration levels. Their condense structures across multiple length scales are studied using small/wide-angle X-ray scattering (S/WAXS) while their hierarchical relaxation dynamics are probed via broadband dielectric spectroscopy (BDS). The spatio-temporal studies combined with molecular dynamics (MD) analysis offer insight into the molecular origin of the water-coupled relaxation dynamics. The water-mediated dynamical transition of POC1 is discovered and we propose it as the fingerprint information of the antifreeze activities, denaturation and water-regulated visco-elasticity and ionic conductivity.

2 Experimental

2.1 Materials

1,3,5-Benzenetricarboxaldehyde, chloroform, dichloromethane (DCM), activated carbon (AC, YP-50F), acetylene black (AB), methanol, poly(vinylidene fluoride) (PVDF), N-methyl-2-pyrrolidone (NMP), and lithium bis(trifluoromethanesulfonyl) imide (LiTFSI) were purchased from Aladdin and used without further purification. Ethylenediamine and Sodium Borohydride were purchased from Guangzhou chemical reagent factory. Deionized water (DI water) was obtained from Milli-Q water purification system. All glassware was washed with alkaline water and rinsed with ethanol.

2.2 Sample preparation

POCs studied in this work were prepared according to reported methods [26, 27]. We label the obtained molecules as POC1 and POC2, according to the flexibility of structure. The dried as-synthesized POC1 is designated as POC1d. POC1 was then separately equilibrated with humid air at 43% RH (relative humidity) and 98% RH, the resulting labeled POC1 we refer to as POC1m and POC1w, respectively. The glassy state of POC1 (POC1g) and POC2 was obtained by heating the sample to the temperature above its inherent T_g, then cooling to room temperature. The crystallization-related scattering peaks of the initial sample disappeared after annealing (Fig. S3 in the Electronic Supplementary Material (ESM)). After the heating-cooling cycle, the as-formed molecular glass POC1g becomes brittle, and is water-free.

3 Results and discussion

The POC1 bulk is sensitive to environmental humidity and their physical appearances can be tuned from brittle glass, elastomer to highly viscos liquid (Fig. 1(d)). The samples treated under different humidity are named as POC1m (43% RH), POC1w (98% RH), and POC1g (fully dried). For gravimetric analysis, their water contents are 8.8%, 42.0% and 0% wt., respectively. As control studies, POC2 possessing similar cage topology but more rigid backbone is also treated at different humidity; however, no obvious change of its physical appearance can be detected (Fig. 1(a) and Fig. S4 in the ESM). It seems that the viscoelasticity and humidity responsiveness of POC1 should be highly dependent on the segmental flexibility of the cage backbones. Meanwhile, the hydrogen bonding (HB) between water ad POC1 works as the physical crosslinker for the promising performance as elastomers while the introduced water serves as the critical structural units rather than just plasticizers (Fig. 1(b)). Actually, in typical molecular dynamics (MD) simulation, seldom direct HB connection between two neighboring cages can be observed while water-mediated connection of the cages is the dominated structures (simulation details are listed in Supporting Information). This is witnessed by the increase in the root mean square deviation (RMSD) of the POC1 carbon structure as the hydration level increases (Figs. S6 and S7 in the ESM).

The framework of POC1 is flexible and the SNPs possess high deformability, leading to the glassy nature of its bulk materials. In the thermal analysis of POC1g, single glass transition process can be observed, which should be originated from the cooperative segment relaxation dynamics of POC1 framework (Fig. 1(c)) [28]. Interestingly, at temperature above the glass transition temperature (T_g), POC1 undergoes an irreversible structural collapse analogous to protein denaturation in salt solution, resulting in hydrophobic aggregated states (Fig. S5 in the ESM). The POC1g sample show broad glass transition range and this implies the non-homogeneous packing of structure in its bulk state. With medium hydration level, the antifreeze activity of POC1m can be confirmed by showing only single glass transition step with the absence of ice melting process. For the highly hydrated POC1w, the glass transition shifts to much lower temperature (T_g ~ −50 °C) while an exothermic peak at −20 °C and an endothermic peak at −7 °C demonstrate the recrystallization of supercooled water and the advanced melting of the confined small ice nuclei. Generally, the T_s of POC1 samples decrease with the increased hydration level, suggesting the plasticizer role of water in the segmental dynamics of POC1. The hydrated POC1s demonstrate higher excess heat capacity at T_g, ΔC_p, than the dehydrated POC1g, confirming the impact of water in the activation of structural dynamics of POC1 framework (Table S1 in the ESM).

The thermal hysteresis behaviors are extensively investigated to gain insight into the anti-freeze properties. The hydrated POC1m and POC1w both show no signs of ice crystallization even with a slow cooling rate of 1 °C·min^{-1} while the ice recrystallization and melting can be observed for POC1w in the reheating cycle (Fig. S8 in the ESM). The water molecules are supercooled and the ice crystallization is effectively suppressed. Due to the comparatively low hydration level of POC1m, the ice crystallization can be completely inhibited. For POC1w, the slow crystallization on cooling is responsible for the failure to resolve the exotherm associated with crystallization. Further temperature resolved WAXS measurements are performed to resolve the true freezing point (T_f) and melting point (T_m) for water in POC1w. Characterized by the ice crystalline peaks in Fig. 1(e), T_f lies between −40 and −30 °C during the cooling process, while T_m lies between −20 and −22 °C

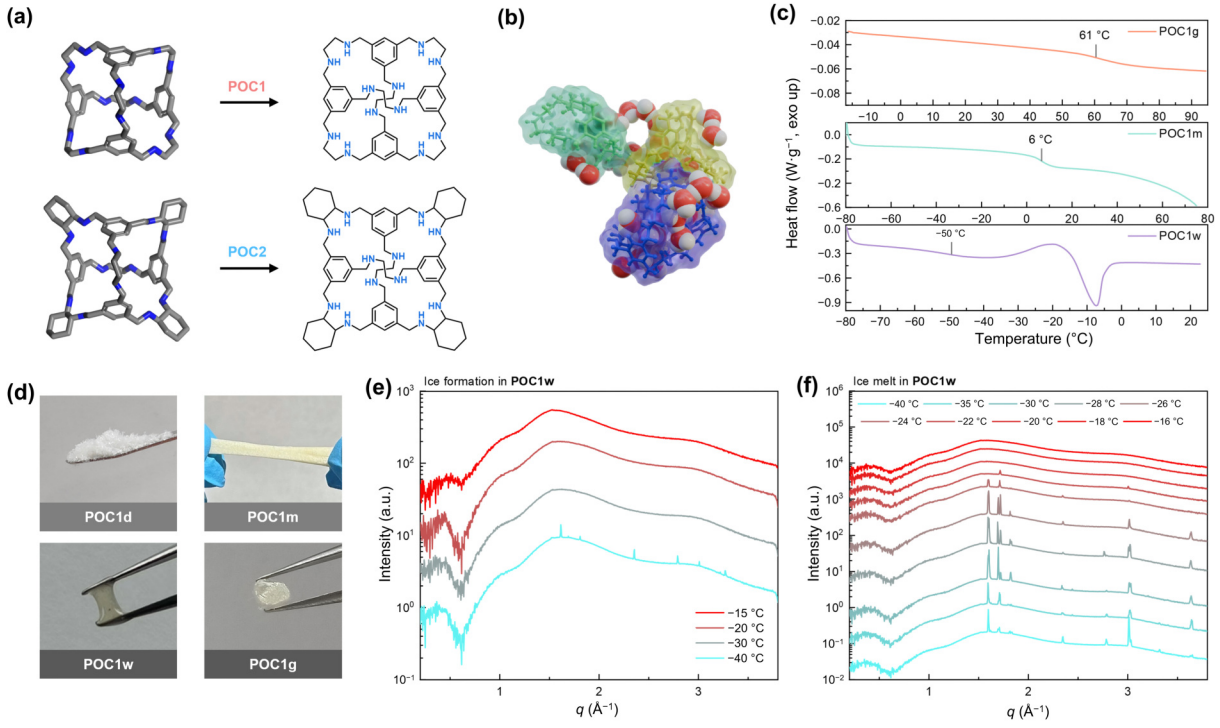

Figure 1 Humidity-tunable mechanical properties and antifreeze activity in flexible cage-based POC1. (a) Chemical structures of POC1/POC2. (b) Example of the simulation result where water chain forms in the nanochannel created by POC1. (c) DSC measurements for POC1 equilibrated in different humidity level with ramping rate of 10 °C·min^{-1}. (d) Photos of the POC1 samples under different humidity conditions. Temperature-resolved WAXS monitoring the (e) freezing and (f) thawing of POC1w with ramping rate of 1 °C·min^{-1}.

in the melting cycle (Fig. 1(f)). The thermal hysteresis $\Delta T = T_m - T_f \approx 15–18$ K, comparable to values observed in some hyperactive antifreeze materials. The large thermal hysteresis gap between T_m and T_f supports the resemblance between POC1 and hyperactive AFPs. Meanwhile, the shape factor of POC1 in the scattering profiles are nearly identical, confirming the robustness of POC1 framework during cooling (Figs. 1(e) and 1(f)). Importantly, temperature resolved WAXS patterns for POC1m show no crystalline ice peaks across the tested range (Fig. S9 in the ESM).

The states of water in POC1 hydrates were further characterized. TGA reveals that POC1w displays two weight-loss steps: one below 100 °C (free/loosely bound water) and another above 100 °C (strongly bound water). In contrast, POC1m shows only a single weight-loss step above 100 °C, indicating that all water is tightly bound (Fig. S10 in the ESM). High-field solid-state ^{1}H NMR spectroscopy provides insights into the dynamic states and molecular environment of water. In the ^{1}H NMR spectrum of POC1m, the water signal is basically buried in the broadened signal at around 5.8 ppm, suggesting the restricted mobility of strongly bound water molecules within the rigid low-hydration matrix. Instead, a sharper and more resolved water peak is present in the ^{1}H NMR spectrum of POC1w, indicating enhanced molecular mobility due to higher degree of hydration and plasticization, which is consistent with the presence of freezable mobile water. The pronounced difference in spectral linewidth supports the conclusion that water in POC1m is in a more strongly bound state (Fig. S11 in the ESM).

Short range ordering can be observed in the glassy POC1s as two broad peaks in the WAXS pattern with *d*-spacings as 4.5 Å (peak 1) and 15.7 Å (peak 2) (Fig. 2(a)). They are attributed to the backbone spacing within one granular cage unit and the stacking spacing of two adjacent cages, respectively. Upon the treatment at elevated temperatures, the intensity of peak 2 decreases drastically, suggesting the deformation of the granular cage during the removal of structural water. The peak intensity approaches an asymptotic region at 140 °C, suggesting the fully elimination of the structural water from the nanoconfined space. Meanwhile, the intensity of peak 1 increases with elevated temperatures, implying more compact stacking of granular cages. After complete dehydration, the POC1g shows no obvious structural changes below T_g (Fig. 2(b)). The peak 1 shifts towards low q as temperature rises beyond T_g, indicating the dilation of cage framework when the structural dynamics is thermally activated. Molecular simulation confirms the key roles of associated water in inflating and supporting the cage framework (Fig. 2(c)). As the confined water is removed, the flexibility of the cage backbones allows the arene face to fold into the cavity for the self-crowding of cage units and this finally leads to influences on the glass transition behavior. The observations also confirm the structural origin of the denaturation of POC1.

The hierarchical relaxation dynamics of the POC1s are probed through dielectric measurements to gain quantitative and microscopic understanding of the anti-freeze properties, denaturation and water-regulated viscoelasticity. All the POC1s demonstrate two distinctive relaxation modes within the observed frequency domain at temperatures well below their systematic glass transition (Fig. 3(a)). For the slow α-relaxation mode, a distinct cross-over can be observed in the temperature dependence of the relaxation time for all the POC1s while the trend at high and low temperature ranges can be described by Vogel–Fulcher–Tammann (VFT) [29] equation and Arrhenius law, respectively (Fig. 3(b)). The cross-over temperatures match with the T_s obtained from

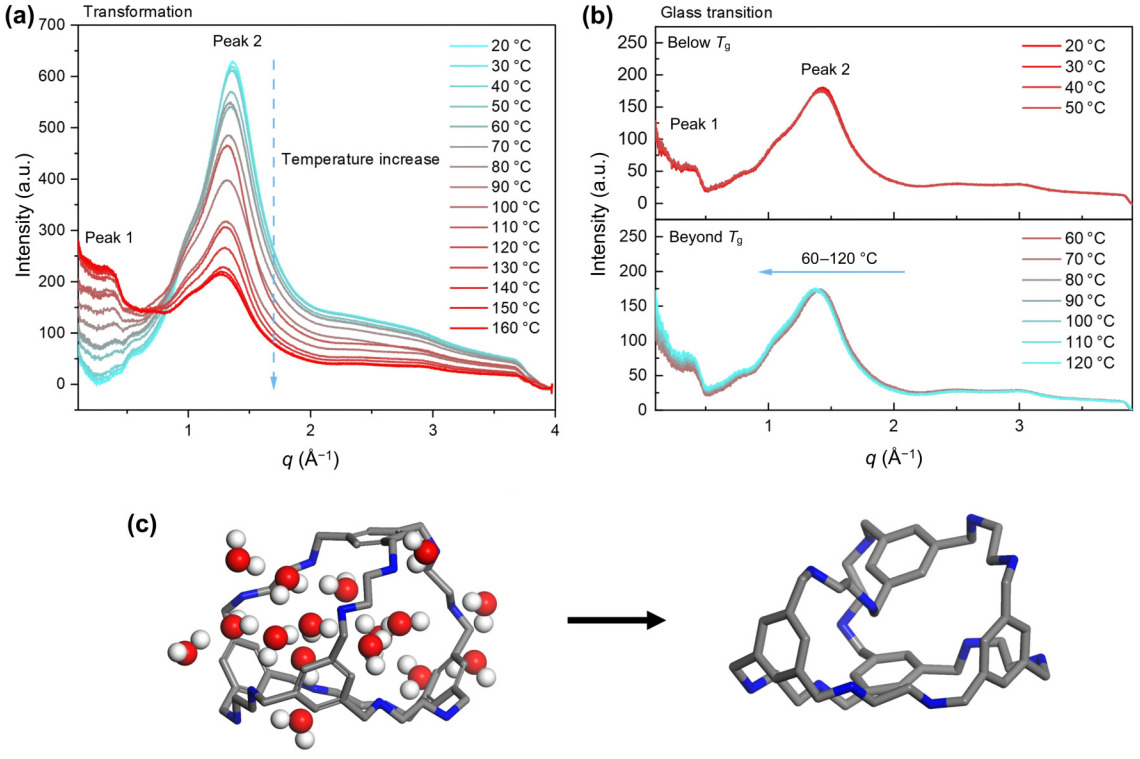

Figure 2 Structural water dictates short-range order and thermally induced deformation in glassy POC1. Temperature-resolved WAXS monitoring (a) the structural transformation from POC1m to POC1g and (b) the glass transition process of POC1g. (c) The difference of architecture between hydrated POC1m and the water-free POC1g.

calorimetric analysis, confirming its same structural origin with glass transition process as the segmental relaxation of the POC1 backbone. The characteristic dynamical transition of POC1s can be located in the 3D plot of electric modulus loss (M'' vs. f vs. T) (Fig. 3(a)) and it is considered as the intrinsic property of the POC1 backbone while water can be used to regulate the transition. It can be conjected that the dynamical transition is related to the fluctuations of the flexible amino segments, while water can associate with the functional groups and drive the onset of dynamics transition. The fast β-relaxation is originated from the intra-cage local dynamics with typical Arrhenius type temperature dependence ($E_{a\beta}$ values shown in Table S2 in the ESM) (Fig. 3(b) and Fig. S15(b) in the ESM). Although β-relaxation is attributed primarily to intra-cage motions, contributions from hydration water reorientation cannot be fully excluded because their time scales partially overlap. The β-relaxation reflects local dynamics strongly coupled to hydration water while the activation energies (Table S2 in the ESM) decrease with hydration due to enhanced local mobility facilitated by these interactions. The dielectric amplitude $\Delta\varepsilon_\beta$ values rise with the increased hydration water contribution (Fig. 3(c)), suggesting water-coupled feature for β relaxation process. This is homologous to the strong coupling of protein localized diffusion with the dynamics of hydration water [30]. Both α- and β-relaxation are rapidly accelerated with the increase of hydration level (Fig. 3(b)), which is consistent with the lowering of T_s due to the increased hydration level. In addition, the γ-relaxation for POC1g is attributed to fast dynamics resulting from localized, non-diffusive motions—such as restricted rotation or vibration of specific molecular groups (Fig. S15(a) in the ESM) [31].

Considering the existence of a substantial fraction of strongly

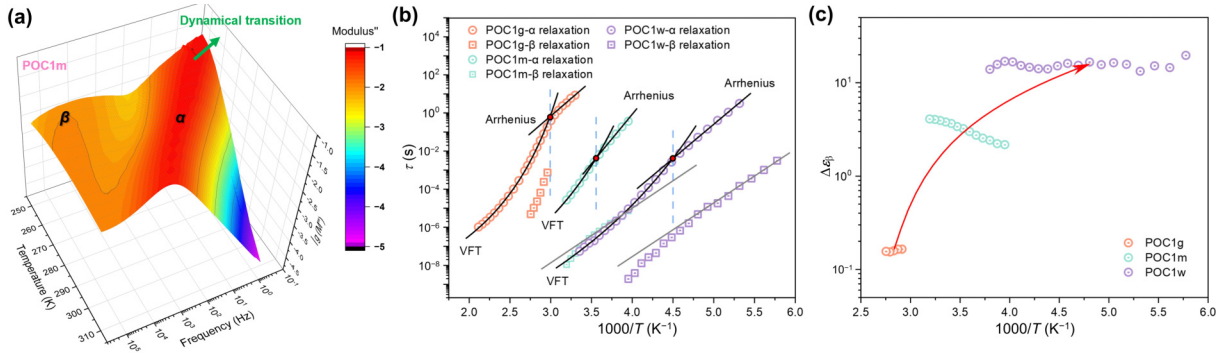

Figure 3 Hierarchical relaxation dynamics and hydration-coupled viscoelasticity in antifreeze POC1 elucidated by BDS. (a) 3D plot of modulus loss versus frequency and temperature for POC1m. (b) Evolution of the relaxation rate as a function of temperature as deduced from BDS experiments for POC1g, POC1m and POC1w. The relaxation time of POC1g, POC1m and POC1w is marked by orange, blue and purple, respectively; while α-relaxation time and β-relaxation time is differentiated by dotted circle and dotted square, separately. (c) Temperature dependence of the dielectric amplitude and $\Delta\varepsilon_\beta$ for processes in POC1g, POC1m and POC1.

bound water even at different hydration levels (Fig. S10 in the ESM), it indicates that water molecules are not merely absorbed as bulk-like plasticizers, but are intimately associated with the POC framework, most likely through hydrogen bonding with amine linkages and confinement within cage cavities and inter-cage nanochannels. Importantly, the bound-water content in POC1m coincides with the absence of ice-melting signatures in DSC and the pronounced enhancement of β-relaxation strength, suggesting that this population of structural water is directly coupled to local cage dynamics. In contrast, the free-water fraction in POC1w contributes to additional thermal events at subzero temperatures but plays a secondary role in governing the intrinsic relaxation processes of the POC backbone. These observations support a non-classical hydration effect in POC1, in which tightly bound water acts as a co-structural and co-dynamic element that facilitates hierarchical relaxation and dynamical transition, rather than serving as a passive diluent as assumed in conventional plasticization models.

An energy landscape analysis of POC1 dynamics is proposed to correlate the conformational fluctuations to its denaturation, anti-freeze properties and water-regulated viscoelasticity (Fig. S15(a) in the ESM) [31, 32]. The α-relaxation can be considered as inter-basin conformational jumps, representing the long-range cooperative motions of POC1 backbones. Similar to most bioactive materials, α-relaxation here is directly involved in POC functions, e.g., denature, glass transition and viscoelasticity [33–35]. Meanwhile, the β-relaxation presents the intra-basin conformational jumps and for POC1, it is the so-called localized diffusion that could be connected to the dynamics of hydration water [36]. According to the mode-coupling theory [37, 38], the β-relaxation is the necessary precursor of the α-relaxation since the ratios between the activation energy of β-relaxations and their T_g, $E_{a,\beta}/RT_g$, satisfies the conditions provided for the Johari-Goldstein β-relaxation (Table S2 in the ESM) [38, 39]. Therefore, as the microscopic understanding of the critical role of water, the friction coefficient of this localized motion (β-relaxation) is determined by the hydration water and internal friction (flexibility). The structural α-relaxation is generated from the propagation of mobility through dynamic facilitation of β-relaxations [40, 41]. In dynamic facilitation theory, localized β-events reduce local energy barriers and trigger cooperative rearrangements in neighboring regions. These cascaded events lead to long-range α-relaxation characteristic of glass-forming systems.

The viscoelastic nature of POC1m confers significant advantages in both processability and versatile applications. The elasticity of POC1m is characterized from typical SAOS and tensile tests (Figs. 4(a) and 4(b)), which shows Young's modulus as 100 MPa and an 180% elongation at break. The water-accelerated dynamics should facilitate the transportation of ions, thereby establishing the promising potential of POC1m for solid-state Li^+ conduction applications. Typical lithium salt, LiTFSI, is molecularly dispersed in POC1 bulk and the simple treatment at 43% RH can simultaneously improve its structural flexibility and ion conductivity from 9.20×10^{-7} (POC1g) to 3.07×10^{-4} S·cm^{-1} (Fig. 4(c)). Meanwhile, the water under the soft nanoconfinement of POC1 show hindered diffusive dynamics and this disfavor water electrolysis for widened electrochemical window (2.5 V) that enables the fabrication of high-density batteries (Fig. 4(d)).

To validate the potential application of POC1m as a solid-state Li^+ conductor, electrochemical tests were conducted by employing POC1m in supercapacitors. Cyclic voltammetry (CV) curves exhibited characteristic rectangular shapes at low scan rates, indicative of charge storage primarily governed by an electric double-layer capacitance (EDLC) mechanism (Fig. 4(e)). GCD measurements further corroborated excellent reversibility, revealing symmetrical triangular profiles across all tested current densities

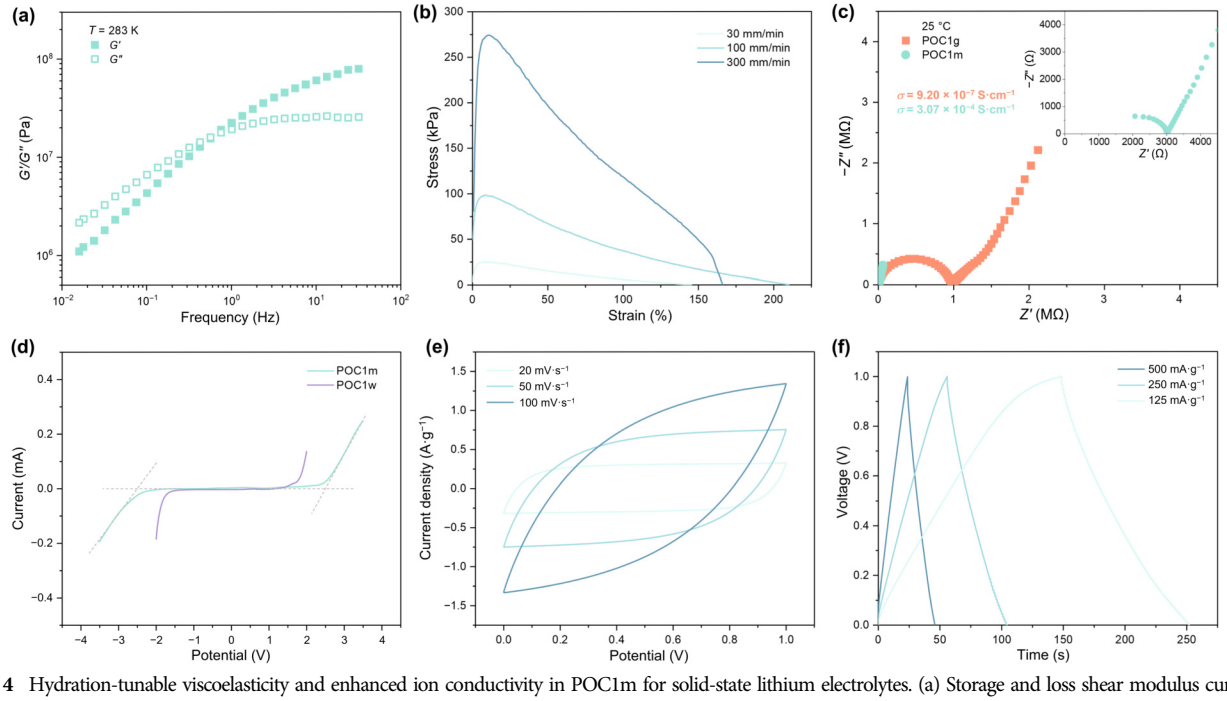

Figure 4 Hydration-tunable viscoelasticity and enhanced ion conductivity in POC1m for solid-state lithium electrolytes. (a) Storage and loss shear modulus curves for POC1m at 283 K. (b) Tensile measurements for POC1m at room temperature with 43% RH flow purged on. (c) EIS of POC1g and POC1m at room temperature. (d) Electrochemical stabilization window (ESW) of POC1m determined by linear sweep voltammetry (LSV). (e) CV curves of the SC at different scan rates at 25 °C. (f) GCD curves of the SC at different current density at 25 °C.

(Fig. 4(f)). The discharge curves demonstrated highly linear relationships, signifying relatively constant capacitance values during discharge—a hallmark of ideal EDLC behavior. In conclusion, POC1m-based supercapacitors with high specific capacity (125 $mA \cdot g^{-1}$, 51.7 $F \cdot g^{-1}$) and good multiplicity confirm the potential application of POC1m as a solid-state Li^+ conductor.

4 Conclusions

In summary, the spatiotemporal studies the POC1 model systems offer quantitative details in regard to its thermodynamics, relaxation dynamics and glassy structures. The acceleration intrinsic relaxation rates in POC1 in a strong hydration dependence is highlighted. The hydration water is coupled strongly with the POC1's backbones and together displays coupling dynamics. The presence of a "dynamical transition" is observed for the same location as the glass transition at the temperature region in its dielectric α-relaxation map. The structure of POC1 undergoes severe distortion during the dehydration and glass transition process and this could be inferred as the structural and kinetic origin of the protein-like denaturation of POC1. It can be concluded that the confined water serves as the driving force in altering the spatio-temporal properties of the whole system. These findings open avenues for designing hydration responsive membranes, anti-freeze coatings, or self-healing ion conductors for flexible electronics operating in humid or subzero environments. Moreover, they not only provide new perspectives and opportunities in biomimicry, but also shed light in the fabrications of functional supramolecular materials with water as key structural units.

Electronic Supplementary Material: Supplementary material (NMR of POC1/POC2, pictures of POC1/POC2, MSD versus relaxation times of hydration water in POC1w, DSC/TGA/WAXS of POC1, the simulated density of POC1 under different temperature, and dielectric investigation of water mediated POC1 dynamics) is available in the online version of this article at https://doi.org/10.26599/NR.2026.94908366.

Data availability

All data needed to support the conclusions in the paper are presented in the manuscript and the Electronic Supplementary Material. Additional data related to this paper may be requested from the corresponding author upon request.

Acknowledgements

We would like to thank the support from BL16B1, BL19U2, and BL10U1 of Shanghai Synchrotron Radiation Facility for the access to the synchrotron-based SAXS. This work was supported by the National Natural Science Foundation of China (Nos. 22241501 and 92261117), the Guangdong-Hong Kong-Macao Joint Laboratory for Neutron Scattering Science and Technology, the Open Fund of the China Spallation Neutron Source Songshan Lake Science City (No. KFKT2023A09), TCL science and technology innovation fund (No. 20222056), and Guangzhou Municipal Science and Technology Bureau (No. 2023A04J1364).

Declaration of competing interest

All the contributing authors report no conflict of interests in this work.

Author contribution statement

P. C. Y. conceived the original idea for the project. L. K. C. and Y. Y. L. synthesized the materials. L. K. C. carried out thermal analysis, X-ray scattering measurements, and relaxation dynamics analysis. W. G. S. carried out electrochemical measurements. J. D. C. conducted mechanical tests. W. Q. Y., X. Y. Y., X. P. C., and X. K. carried out MD simulation. L. K.C., W. G. S., and P. C. Y. analyzed all the data and wrote the manuscript.

Use of AI statement

None.

References

[1] Cerveny, S.; Mallamace, F.; Swenson, J.; Vogel, M.; Xu, L. M. Confined water as model of supercooled water. *Chem. Rev.* **2016**, *116*, 7608–7625.
[2] Ball, P. Water as an active constituent in cell biology. *Chem. Rev.* **2008**, *108*, 74–108.
[3] Ball, P. Water is an active matrix of life for cell and molecular biology. *Proc. Natl. Acad. Sci. USA* **2017**, *114*, 13327–13335.
[4] Dargaville, B. L.; Hutmacher, D. W. Water as the often neglected medium at the interface between materials and biology. *Nat. Commun.* **2022**, *13*, 4222.
[5] Laage, D.; Elsaesser, T.; Hynes, J. T. Water dynamics in the hydration shells of biomolecules. *Chem. Rev.* **2017**, *117*, 10694–10725.
[6] Petridis, L.; O'Neill, H. M.; Johnsen, M.; Fan, B. X.; Schulz, R.; Mamontov, E.; Maranas, J.; Langan, P.; Smith, J. C. Hydration control of the mechanical and dynamical properties of cellulose. *Biomacromolecules* **2014**, *15*, 4152–4159.
[7] Grommet, A. B.; Feller, M.; Klajn, R. Chemical reactivity under nanoconfinement. *Nat. Nanotechnol.* **2020**, *15*, 256–271.
[8] Fomina, M.; Schirò, G.; Cupane, A. Hydration dependence of myoglobin dynamics studied with elastic neutron scattering, differential scanning calorimetry and broadband dielectric spectroscopy. *Biophys. Chem.* **2014**, *185*, 25–31.
[9] Salvati Manni, L.; Assenza, S.; Duss, M.; Vallooran, J. J.; Juranyi, F.; Jurt, S.; Zerbe, O.; Landau, E. M.; Mezzenga, R. Soft biomimetic nanoconfinement promotes amorphous water over ice. *Nat. Nanotechnol.* **2019**, *14*, 609–615.
[10] Shin, Y.; Brangwynne, C. P. Liquid phase condensation in cell physiology and disease. *Science* **2017**, *357*, eaaf4382.
[11] Marshall, C. B.; Fletcher, G. L.; Davies, P. L. Hyperactive antifreeze protein in a fish. *Nature* **2004**, *429*, 153–153.
[12] Hudait, A.; Moberg, D. R.; Qiu, Y. Q.; Odendahl, N.; Paesani, F.; Molinero, V. Preordering of water is not needed for ice recognition by hyperactive antifreeze proteins. *Proc. Natl. Acad. Sci. USA* **2018**, *115*, 8266–8271.
[13] Sun, T. J.; Lin, F. H.; Campbell, R. L.; Allingham, J. S.; Davies, P. L. An antifreeze protein folds with an interior network of more than 400 semi-clathrate waters. *Science* **2014**, *343*, 795–798.
[14] Dong, S. Y.; Leng, J.; Feng, Y. X.; Liu, M.; Stackhouse, C. J.; Schönhals, A.; Chiappisi, L.; Gao, L. Y.; Chen, W.; Shang, J. et al. Structural water as an essential comonomer in supramolecular polymerization. *Sci. Adv.* **2017**, *3*, eaao0900.
[15] Van Zee, N. J.; Adelizzi, B.; Mabesoone, M. F. J.; Meng, X.; Aloi, A.; Zha, R. H.; Lutz, M.; Filot, I. A. W.; Palmans, A. R. A.; Meijer, E. W. Potential enthalpic energy of water in oils exploited to control supramolecular structure. *Nature* **2018**, *558*, 100–103.
[16] Yeh, Y.; Feeney, R. E. Antifreeze proteins: Structures and mechanisms of function. *Chem. Rev.* **1996**, *96*, 601–618.
[17] Perrin, A.; Musa, O. M.; Steed, J. W. The chemistry of low dosage clathrate hydrate inhibitors. *Chem. Soc. Rev.* **2013**, *42*, 1996–2015.

[18] Liu, K.; Wang, C. L.; Ma, J.; Shi, G. S.; Yao, X.; Fang, H. P.; Song, Y. L.; Wang, J. J. Janus effect of antifreeze proteins on ice nucleation. *Proc. Natl. Acad. Sci. USA* **2016**, *113*, 14739–14744.
[19] Zhong, D. P.; Pal, S. K.; Zewail, A. H. Biological water: A critique. *Chem. Phys. Lett.* **2011**, *503*, 1–11.
[20] Yuan, Y. D.; Dong, J. Q.; Liu, J.; Zhao, D. H.; Wu, H.; Zhou, W.; Gan, H. X.; Tong, Y. W.; Jiang, J. W.; Zhao, D. Porous organic cages as synthetic water channels. *Nat. Commun.* **2020**, *11*, 4927.
[21] Tozawa, T.; Jones, J. T. A.; Swamy, S. I.; Jiang, S.; Adams, D. J.; Shakespeare, S.; Clowes, R.; Bradshaw, D.; Hasell, T.; Chong, S. Y. et al. Porous organic cages. *Nat. Mater.* **2009**, *8*, 973–978.
[22] Liu, M.; Zhang, L. D.; Little, M. A.; Kapil, V.; Ceriotti, M.; Yang, S. Y.; Ding, L. F.; Holden, D. L.; Balderas-Xicohténcatl, R.; He, D. L. et al. Barely porous organic cages for hydrogen isotope separation. *Science* **2019**, *366*, 613–620.
[23] Hasell, T.; Schmidtmann, M.; Stone, C. A.; Smith, M. W.; Cooper, A. I. Reversible water uptake by a stable imine-based porous organic cage. *Chem. Commun.* **2012**, *48*, 4689–4691.
[24] Liu, M.; Little, M. A.; Jelfs, K. E.; Jones, J. T. A.; Schmidtmann, M.; Chong, S. Y.; Hasell, T.; Cooper, A. I. Acid- and base-stable porous organic cages: Shape persistence and pH stability via post-synthetic "tying" of a flexible amine cage. *J. Am. Chem. Soc.* **2014**, *136*, 7583–7586.
[25] Liu, M.; Chen, L. J.; Lewis, S.; Chong, S. Y.; Little, M. A.; Hasell, T.; Aldous, I. M.; Brown, C. M.; Smith, M. W.; Morrison, C. A. et al. Three-dimensional protonic conductivity in porous organic cage solids. *Nat. Commun.* **2016**, *7*, 12750.
[26] Culshaw, J. L.; Cheng, G.; Schmidtmann, M.; Hasell, T.; Liu, M.; Adams, D. J.; Cooper, A. I. Dodecaamide cages: Organic 12-arm building blocks for supramolecular chemistry. *J. Am. Chem. Soc.* **2013**, *135*, 10007–10010.
[27] Lydon, D. P.; Campbell, N. L.; Adams, D. J.; Cooper, A. I. Scalable synthesis for porous organic cages. *Synth. Commun.* **2011**, *41*, 2146–2151.
[28] Molak, A.; Paluch, M.; Pawlus, S.; Klimontko, J.; Ujma, Z.; Gruszka, I. Electric modulus approach to the analysis of electric relaxation in highly conducting $(Na_{0.75}Bi_{0.25})(Mn_{0.25}Nb_{0.75})O_3$ ceramics. *J. Phys. D: Appl. Phys.* **2005**, *38*, 1450–1460.
[29] Garca-Coln, L. S.; del Castillo, L. F.; Goldstein, P. Theoretical basis for the Vogel-Fulcher-Tammann equation. *Phys. Rev. B* **1989**, *40*, 7040–7044.
[30] Schirò, G.; Fichou, Y.; Gallat, F. X.; Wood, K.; Gabel, F.; Moulin, M.; Härtlein, M.; Heyden, M.; Colletier, J. P.; Orecchini, A. et al. Translational diffusion of hydration water correlates with functional motions in folded and intrinsically disordered proteins. *Nat. Commun.* **2015**, *6*, 6490.
[31] Khodadadi, S.; Sokolov, A. P. Atomistic details of protein dynamics and the role of hydration water. *Biochim. Biophys. Acta Gen. Subj.* **2017**, *1861*, 3546–3552.
[32] Khodadadi, S.; Sokolov, A. P. Protein dynamics: From rattling in a cage to structural relaxation. *Soft Matter* **2015**, *11*, 4984–4998.
[33] Hansen, J. S.; Kisliuk, A.; Sokolov, A. P.; Gainaru, C. Identification of structural relaxation in the dielectric response of water. *Phys. Rev. Lett.* **2016**, *116*, 237601.
[34] Meister, K.; Ebbinghaus, S.; Xu, Y.; Duman, J. G.; DeVries, A.; Gruebele, M.; Leitner, D. M.; Havenith, M. Long-range protein-water dynamics in hyperactive insect antifreeze proteins. *Proc. Natl. Acad. Sci. USA* **2013**, *110*, 1617–1622.
[35] Salvi, N.; Abyzov, A.; Blackledge, M. Solvent-dependent segmental dynamics in intrinsically disordered proteins. *Sci. Adv.* **2019**, *5*, eaax2348.
[36] Hong, L.; Smolin, N.; Lindner, B.; Sokolov, A. P.; Smith, J. C. Three classes of motion in the dynamic neutron-scattering susceptibility of a globular protein. *Phys. Rev. Lett.* **2011**, *107*, 148102.
[37] Nogales, A.; Sanz, A.; Ezquerra, T. A. On the role of the β process as precursor of the α relaxation in aromatic polyesters. *J. Non-Cryst. Solids* **2006**, *352*, 4649–4655.
[38] Ngai, K.; Capaccioli, S. Relation between the activation energy of the Johari–Goldstein β relaxation and T_g of glass formers. *Phys. Rev. E* **2004**, *69*, 031501.
[39] Paluch, M.; Roland, C. M.; Pawlus, S.; Zioło, J.; Ngai, K. L. Does the Arrhenius temperature dependence of the Johari-Goldstein relaxation persist above T_g. *Phys. Rev. Lett.* **2003**, *91*, 115701.
[40] Baker, D. L.; Reynolds, M.; Masurel, R.; Olmsted, P. D.; Mattsson, J. Cooperative intramolecular dynamics control the chain-length-dependent glass transition in polymers. *Phys. Rev. X* **2022**, *12*, 021047.
[41] Keys, A. S.; Hedges, L. O.; Garrahan, J. P.; Glotzer, S. C.; Chandler, D. Excitations are localized and relaxation is hierarchical in glass-forming liquids. *Phys. Rev. X* **2011**, *1*, 021013.